Closed-Form Expressions for ICI/ISI in Filtered OFDM Systems for Asynchronous 5G Uplink

Closed-Form Expressions for ICI/ISI in Filtered OFDM Systems for Asynchronous 5G Uplink

Shendi Wang, *Student Member,* John S. Thompson, *Fellow, IEEE,*
and Peter M. Grant, *Fellow, IEEE*

***Abstract*—One of the major purposes for fifth generation (5G) communications waveform design is to relax the synchronisation requirements for supporting efficient massive machine type communications (MTC). Polynomial cancellation coded orthogonal frequency-division multiplexing (PCC-OFDM) and universal filtered multi-carrier (UFMC) are designed to reduce the side-lobes of the orthogonal frequency division multiplexing (OFDM) waveform to protect against intercarrier interference (ICI) in the 5G uplink. To the best of our knowledge, there is no analysis of the effect of ICI for the UFMC system with time offset transmissions that many arise in MTC scenarios. Furthermore, there is no study on reducing the computational complexity of the UFMC system. This paper provides closed-form expressions for time offsets interference in such a case for OFDM, PCC-OFDM and UFMC. This paper also presents theoretical analysis for the signal-to-interference-plus-noise ratio (SINR), achievable rate and bit error ratio (BER) performance. The results show that PCC-OFDM significantly protects against ICI at the cost of halving the spectral efficiency. UFMC improves the ICI and intersymbol interference (ISI) protection performance, especially when the length of time offset is very small, at the cost of significantly increasing the computational complexity. Finally, this paper proposes the overlap and add UFMC (OA-UFMC) and a variant of UFMC using infinite impulse response prototype filter banks (IIR-UFMC) to reduce the processing complexity.**

I. Introduction

WIRELESS communications researchers are developing a vision for beyond the long-term evolution (LTE), or the fourth generation of wireless communication systems (4G), to enable the roll-out of the fifth generation (5G) standard [1], [2], which will support both human-centric and machine type communications (MTC) [3]. In addition, 5G wireless communication systems will have to be able to deal with a very diverse variety of traffic types ranging from regular high-rate traffic (e.g., mobile data downloading applications), sporadic low data rates (e.g., smart meters) and urgent low latency transmissions (e.g., real time vehicle traffic information) [4].

Orthogonal frequency division multiplexing (OFDM) has been widely used in 4G [5]. However, there are several challenging problems in the application of OFDM cellular systems to support a large number of MTC devices in the 5G uplink. First, in OFDM, the orthogonality is based on strict synchronisation between each sub-carrier, and as soon as the orthogonality is destroyed by multi-cell or multiple access transmission or through time offsets between transmitters, interference between sub-carriers can become significant [6]. This is due to the Dirichlet kernel $\sin(Nx)/\sin(x)$ used in OFDM, which quickly approaches the $\mathrm{sinc}(x)$ kernel for a large number of sub-carriers (N). For such a kernel, the amplification of small errors (e.g., due to the time or frequency offsets) is not independent of N and can grow with order $(\log N)$ [6]. Second, one significant design goal for 5G is to be able to support efficiently multiple traffic types. It should be able to deal with both high and low volume data transmission requirements and support both synchronous and asynchronous transmissions [4]. In LTE, the uplink users have to be synchronised. The terminal devices measure the time delay from the base station (BS) and try to adjust their uplink transmissions to compensate for the delay in the downlink. The 5G systems might need simplification for handling the MTC transmissions. They should not have to compensate the timing offsets. Third, one key aspect of user-centric processing is for devices to be connected to multiple base stations simultaneously [7]. The dynamic changes in distance between the devices and base stations require a flexible synchronised processing environment. Thus tight synchronisation, as required in LTE, appears not to be cost-effective or even possible for a multi-user 5G system which is supporting thousands of subscribers in one cell [7]. Relaxing the synchronism requirements can significantly improve operational capabilities, bandwidth efficiency and even battery lifetime particularly when supporting low data rate MTC devices [6].

A. Motivation and Related Work

In order to relax the synchronisation requirements, there are several approaches to deal with asynchronous and non-orthogonal transmission, to reduce the side-lobe levels of the waveform and minimise intersymbol interference (ISI) and intercarrier interference (ICI).

First, polynomial cancellation coded orthogonal frequency-division multiplexing (PCC-OFDM) [8] is a frequency coding technique in which the data to be transmitted is mapped onto weighted groups of sub-carriers. PCC-OFDM has been shown to be much less sensitive than for OFDM to frequency offset and Doppler spread but the spectral efficiency is at best approximately half of that for OFDM as each data symbol is mapped to at least two sub-carriers [8]. Second, filter bank multi-carrier (FBMC) is designed with a prototype filter which improves frequency selectivity. Separation of each sub-carrier through a filtering process also avoids the need for any timing synchronisation between the users [9]. If a filter is designed for each sub-carrier in FBMC, the filter impulse response length could be very long, which increases the symbol duration. Practically, this significantly increases the computational complexity, which mitigates against achieving

a low cost 5G implementation. Third, universal filtered multi-carrier (UFMC) [6], an alternative version of FBMC, groups a number of sub-carriers into a sub-band and passes the sub-band signal though a narrow sub-band finite impulse response (FIR) filter. Compared with FBMC, the processing complexity of UFMC is significantly reduced [10], but our previous paper [11] has shown that the complexity is still much higher than OFDM. Fourth, weighted overlap and add (WOLA)-OFDM is a filtered cyclic prefix (CP) CP-OFDM waveform proposed for 3GPP in [12], which is a similar to UFMC. WOLA overlaps several samples together between the nearby time domain filtered signals to reduce the transmitted signal length. However, [12] has shown that WOLA has an inferior side-lobe reduction performance compared to UFMC while requiring a similar level of complexity due to the filter bank requirement.

B. Contributions

Previous studies have performed several comparison simulations to assess the achievable UFMC side-lobe reduction performance [13]–[15]. However, there is no paper on reducing the computational complexity for UFMC or for developing closed-form expressions for ICI and ISI in a UFMC time offset system. Moreover, there is not a detailed analysis and comparison between CP-OFDM, PCC-OFDM and UFMC waveforms to measure the overall time offset performance. The main contributions in this paper can be summarised as follows:

1) Propose two novel techniques, which are the overlap and add UFMC (OA-UFMC) and the analogue infinite impulse response (IIR) filters (IIR-UFMC).
2) Both OA-UFMC and IIR-UFMC can provide similar system performance compared with UFMC and with the benefit of significantly reducing the computational complexity of the inverse fast Fourier transform (IFFT).
3) Derive closed-form expressions for the intercarrier interference caused by time offsets between adjacent asynchronous MTC users and the intersymbol interference caused by the multipath channel. First, our expressions can be easily used to compute the signal-to-interference-plus-noise ratio (SINR), the achievable rate and the bit error ratio (BER). Second, our closed-form expressions can be used in both additive white Gaussian noise and multipath transmission scenarios.
4) Provide a detailed system comparison and analysis for different filter designs, considering power spectral density (PSD), SINR, achievable rate, BER, computational complexity and peak-to-average power ratio (PAPR) . We also measure the time offset performance when varying the number of zero sub-carriers between adjacent users.
5) Provide a framework for the trade-off between the system performance and the computational complexity, which helps system designers to balance these parameters.

The rest of this paper is organised as follows. Section II introduces the state of the art. Section III proposes the OA-UFMC and IIR-UFMC systems, and analyses the computational complexity. In Section IV, a time offset model is provided and the interference is analysed. Section V presents the numerical results and Section VI concludes the paper. In this paper, $\mathbb{E}[\cdot]$ the expectation operation, $\otimes$ represents the convolution operation and $(\cdot)^*$ the complex conjugate operation.

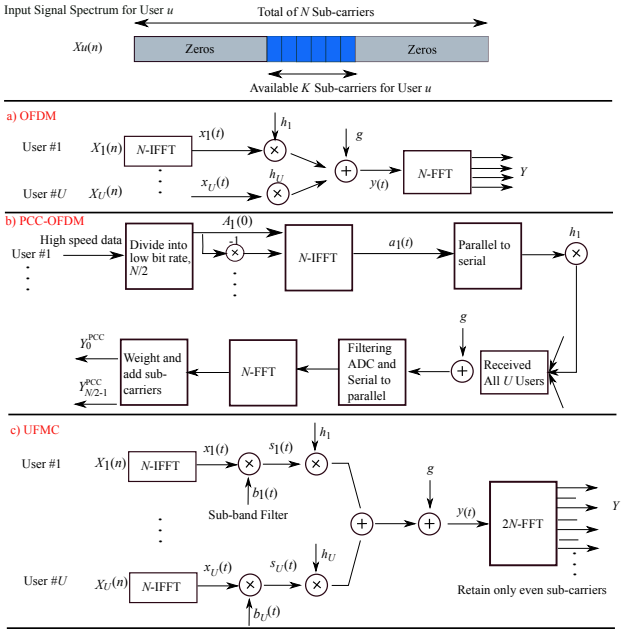

Fig. 1. Multi-user Uplink Transmission Models for (a) OFDM, (b) PCC-OFDM and (c) UFMC.

II. State of the Art

This section introduces the uplink scenario and the 3 basic candidate waveforms including OFDM, PCC-OFDM and UFMC transmission models. We focus on the effect of poor time synchronisation on the ICI experienced in such systems.

A. Uplink Model

We start with a simple uplink system as shown in Fig. 1. There are U users, which are allocated to different carrier frequencies and they transmit simultaneously to a BS. There are a total of N sub-carriers, which are divided among U users in sub-bands. Each user has a total of K available sub-carriers. Here we define L_{CP} as the length of the cyclic prefix (CP) in samples. Then the BS will receive the sum of all the transmitted signals and process it to decode the messages for all U users.

B. OFDM Transmission Model

Assume that $X_u(n)$ denotes that modulation symbol to be transmitted on the nth sub-carrier by the uth user as shown in Fig. 1(a). The baseband OFDM data signal at the output of the N-point IFFT and after adding the CP can be expressed as:

$$x_u(t) = \frac{1}{\sqrt{N}} \sum_{n=0}^{N-1} X_u(n) \cdot e^{j2\pi nt/N}, \qquad (1)$$

where X is the fast Fourier transform (FFT) of x. A wireless Rayleigh multipath channel impulse response h with L_{H} taps is defined as:

$$h_u(t) = \sum_{l_{\mathrm{H}}=0}^{L_{\mathrm{H}}-1} h_{u,l_{\mathrm{H}}} \cdot \delta(t - l_{\mathrm{H}} T_{\mathrm{s}}), \tag{2}$$

where T_{s} is the sample period and $\delta(t)$ is the Dirac delta function and each channel tap l_{H} follows the quasi-static Rayleigh distribution. Note that to simplify our analysis, we assume the number of channel taps L_{H} for each user is the same. Then the received signal over the multipath channel h in the presence of additive white Gaussian noise (AWGN), $g(t)$, can be defined as:

$$y(t) = \sum_{u=1}^{U} x_u(t) \otimes h_u(t) + g(t), \tag{3}$$

where a power spectral density $\sigma^2 = N_0/2$ is assumed for the noise samples $g(t)$.

C. PCC-OFDM Transmission Model

PCC is a frequency coding technique for OFDM in which the data to be transmitted is mapped onto weighted groups of sub-carriers. Reference [8] has shown PCC-OFDM to be much less sensitive than OFDM to frequency offset and Doppler spread. The block diagram of a PCC-OFDM system is shown in Fig. 1(b), where the baseband symbols for the uth user $A_u(0)...A_u(N/2-1)$ will pass through a PCC-OFDM modulator. In this case, pairs of sub-carriers have a relative weighting of $+1$, -1, and the input IFFT signal is organised as $A_u(0), -A_u(0)..., A_u(N/2-1), -A_u(N/2-1)$. After the N-point IFFT, the time domain samples for the u^{th} user $a_u(t)$ can be expressed as:

$$a_u(t) = \frac{1}{\sqrt{N}} \sum_{n=0}^{N-1} A(n) \cdot e^{j2\pi nt/N}. \tag{4}$$

The received signal over the Rayleigh multipath fading channel is then expressed as:

$$v^{\mathrm{PCC}}(t) = \sum_{u=1}^{U} a_u(t) \otimes h_u(t) + g(t). \tag{5}$$

At the receiver, the data is recovered from the FFT outputs, $V^{\mathrm{PCC}}(0)...V^{\mathrm{PCC}}(N-1)$. The mapping of data onto pairs of sub-carriers indicate that the ICI caused by one sub-carrier is substantially cancelled by the ICI caused by the other sub-carrier in the pair. Therefore, in the receiver, pairs of sub-carriers are combined by applying the weightings and then summation:

$$Y^{\mathrm{PCC}}(n) = \frac{V^{\mathrm{PCC}}(2n) - V^{\mathrm{PCC}}(2n+1)}{2}, \ n \in [0, N/2-1]. \tag{6}$$

D. UFMC Transmission Model

The block diagram of standard UFMC [7] is shown in Fig. 1(c). Unlike OFDM, the principle of UFMC is passing each sub-band signal through a narrow band filter. Here we define the bandpass filter impulse response as $b_u(t)$ with the number of filter taps denoted as L_{F}. Then, the time domain UFMC signal at the output of the filter can be expressed as $s_u(t)$:

$$s_u(t) = \frac{1}{\sqrt{N}} \sum_{n=0}^{N-1} X_u(n) e^{j2\pi nt/N} \otimes b_u(t), \ t \in [0, L-1]. \tag{7}$$

In order to provide a fair comparison, we assume the length of the transmitted samples is equal L, which means the $(L = N + L_{\mathrm{F}} - 1)$ should be equal to $(L = N + L_{\mathrm{CP}})$ in terms of the time domain convolution operation. Note that each sub-band filter is designed as a bandpass filter, and then we design each filter's centre frequency to match the sub-band's (or user's) centre frequency. The received signal will be passed though a $2N$-point FFT to convert the time domain signal into the frequency domain. Then, we retain only even sub-carriers whose frequencies correspond to those of the transmitted data carriers [7].

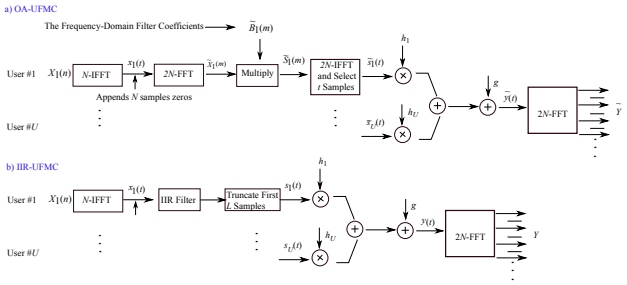

Fig. 2. Block Diagrams for (a) OA-UFMC and (b) IIR-UFMC.

III. Improvement in the Computational Complexity of UFMC

As mentioned above, one of the drawbacks of UFMC is that the computational complexity is significantly increased by applying digital FIR filters to achieve a faster frequency roll-off than is required in CP-OFDM. Higher computational complexity directly increases the number of multiplication operations and raises the energy costs, which does not match the desire to achieve energy efficient 5G MTC terminals. Thus, we propose the OA-UFMC system by applying the multiplication operation in the frequency domain in place of time domain convolution. We also propose the IIR-UFMC which makes use of IIR prototype filter banks. This section will now analyse the computational complexity for those two methods and compare them with standard UFMC, PCC-OFDM and OFDM approaches.

A. Overlap and Add UFMC (OA-UFMC) Model

The block diagram of OA-UFMC is shown in Fig. 2(a), using the overlap and add technique [16] instead of the time domain convolution operation. We increase the number of samples in the frequency domain by using a $2N$-point FFT and then multiply carrier-by-carrier with the frequency-domain filter coefficients. The OA-UFMC system transmission processing is shown in Algorithm 1 with a 5 step process.

Algorithm 1 ***OA-UFMC Transmission Steps***

Step 1: The baseband signal $X_u(n)$ passes through the N-point IFFT block, $x_u(t)$
Step 2: Append N sample zeros on to x_u to obtain $x_u(t^{\mathrm{OA}})$, $t^{\mathrm{OA}} \in [0, 2N-1]$
Step 3: Passes $x_u(t^{\mathrm{OA}})$ through the $2N$-point FFT block, $\tilde{X}_u(m)$
Step 4: Multiplication $\tilde{S}_u(m) = \tilde{X}_u(m) \cdot \tilde{B}_u(m)$, $m \in [0, L-1]$
Step 5: The baseband signal $\tilde{S}_u(m)$ then passes through the $2N$-point IFFT block

Note that there is a good reason why we do not implement directly the product $(X_u(n) \cdot B_u(n))$, where $B_u(n)$ is the N-point FFT of $b_u(t)$. This is because we need to ensure that the transmitted samples are exactly the same length as $s_u(t)$ in equation (7), i.e. with a length of L samples. The signal after the $2N$-point FFT block in the frequency domain can then be expressed as:

$$\tilde{X}_u(m) = \sum_{m=0}^{2N-1} x_u(t^{\mathrm{OA}}) e^{-j2\pi t^{\mathrm{OA}} m/2N}, \tag{8}$$

thus, frequency domain multiplication processing can be expressed as:

$$\tilde{S}_u(m) = \tilde{X}_u(m) \cdot \tilde{B}_u(m), \ m \in [0, L-1], \tag{9}$$

where $\tilde{B}_u(m)$ is the first L samples of the $2N$-point FFT of $b_u(t)$. After transforming $\tilde{S}_u(m)$ into the time domain through the $2N$-point IFFT, we select the first L samples to achieve the same time domain sequence as:

$$\tilde{s}_u(t) = s_u(t), \ t \in [0, L-1]. \tag{10}$$

B. IIR-UFMC

In this paper, we use IIR prototype filters instead of the FIR to reduce the processing cost. The block diagram of IIR-UFMC is shown in Fig. 2(b). Unlike linear phase FIR filters, the phase characteristic of the IIR filter is not linear [17], which can cause a signal distortion. For this reason, we design the cut-off frequency to be wider than the sub-band bandwidth to achieve an almost linear phase in the passband. The processing steps of IIR-UFMC is shown in Algorithm 2.

Algorithm 2 ***IIR-UFMC Transmission Steps***

Step 1: The baseband signal $X(n)$ passes through the N-point IFFT into the time domain
Step 2: Time domain signal passes through a narrow band IIR filter
Step 3: Truncate to the first L samples of the IIR filter output to match to $s_u(t)$, equation (7)
Step 4: Transmit through the wireless channel

C. Computational Complexity Analysis

The main computational complexity is dominated by the number of multiplication operations that are performed. Thus, the computational complexity equations for the UFMC transmitter can be written as Γ^{UFMC}:

$$\Gamma^{\mathrm{UFMC}} = \underbrace{\frac{N}{2}\log_2(N)}_{N\text{–point IFFT}} + (N \cdot L_{\mathrm{F}}), \tag{11}$$

where the term $(N \cdot L_F)$ determines the number of multiplications during the time domain convolution operation. The computational complexity for the OA-UFMC transmitter can be written as Γ^{OA}:

$$\begin{aligned}\Gamma^{\mathrm{OA}} &= \underbrace{\frac{N}{2}\log_2(N)}_{N\text{–point IFFT}} + \underbrace{2\frac{2N}{2}\log_2(2\cdot N)}_{2N\text{–point FFT + }2N\text{–point IFFT}} + L \\ &= \frac{N}{2}\log_2(N) + 2N\left(1+\log_2(N)\right) + N + L_{\mathrm{F}} - 1 \\ &= \frac{5N}{2}\log_2(N) + 3N + L_{\mathrm{F}} - 1. \end{aligned} \tag{12}$$

Compared with UFMC, OA-UFMC can reduce the computational complexity by:

$$\Gamma^{\mathrm{OA}} - \Gamma^{\mathrm{UFMC}} = (L_{\mathrm{F}} - 3)N - 2N\log_2(N) - L_{\mathrm{F}} + 1, \tag{13}$$

operations, and the benefit increases with increasing L_{F}.

This paper also considers IIR filters, such as Chebyshev Type I [18], to determine the ICI performance in terms of reducing the computational complexity caused by the time domain convolution operation. IIR prototype filters with a low filter order, L_{Or}, can achieve a similar performance compared to FIR filter, i.e. $L_{\mathrm{Or}} = 4$. If we consider the IIR filter with the Direct Form I [19], the overall filter coefficients (both feedforward and feedback) is $(2L_{\mathrm{Or}}+1)$. Thus, in this case, the computational complexity for IIR-UFMC can be significantly reduced to:

$$\Gamma^{\mathrm{IIR-UFMC}} = \underbrace{\frac{N}{2}\log_2(N)}_{N\text{–point IFFT}} + \underbrace{L\cdot(2L_{\mathrm{Or}}+1),}_{L\text{ samples and IIR process}} \quad L_{\mathrm{Or}} < L_{\mathrm{F}}. \tag{14}$$

Due to a similar processing required for both PCC-OFDM and CP-OFDM, the N-point IFFT computational complexity can be expressed as:

$$\Gamma^{\mathrm{CP/PCC-OFDM}} = \frac{N}{2}\log_2(N). \tag{15}$$

IV. Time Offset Interference Analysis

The time domain signal of UFMC and OA-UFMC are very similar as shown in (10). This paper considers CP-OFDM (CP-OFDM processing is very similar to PCC-OFDM as both of them add a CP guard interval [8]) and UFMC for the interference analysis. In this section, we use a simple time offset model to analyse the interference caused by asynchronism and also consider the ISI for a longer channel impulse response.

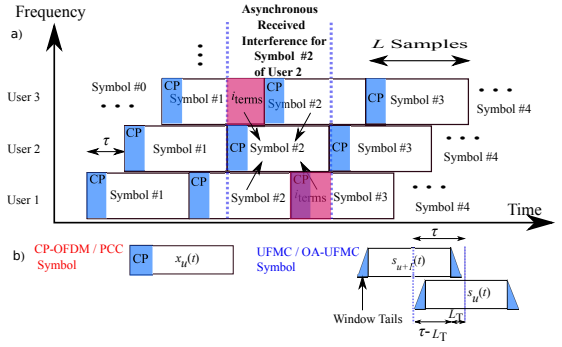

Fig. 3. (a) Time-Frequency Representation of the Time Offset Interference Model, (b) Time Domain Waveforms for CP/PCC-OFDM and UFMC.

A. Time offset Model

We assume that the received MTC signals from the U users are asynchronous and suffer from time offsets at the base station. The time-frequency representation for time offset is shown in Fig. 3(a). To simplify our analysis we start by considering $U = 3$ users where each user transmits 3 OFDM symbols. The scalar τ is the relative delay in timing samples between adjacent users. In addition, we assume that the time offsets between each pair of adjacent users are the same. This paper focuses on decoding the 2nd OFDM symbol for each user. Here we define #1, #2 and #3 as the 1st, 2nd and 3th OFDM symbol following the notation in Fig. 3(a).

B. ICI Analysis Caused by Time Offset

This subsection analyses the ICI interference for both the CP/PCC-OFDM and UFMC systems.

1) CP-OFDM (or PCC-OFDM) System ICI Analysis: The ICI interference for each user is caused by the OFDM side-lobes of the adjacent asynchronous users. As shown in Fig. 3(a), the interference terms for the 2nd symbol of user 2, $x_2^{\#2}(t)$, are separated into four parts: two of the terms arise from the adjacent time periods and two of them arise from the same time period. First, the interference to $x_2^{\#2}(t)$ from the adjacent time periods is dominated by the first τ samples from $x_1^{\#3}(t)$ and the tail τ samples from $x_3^{\#1}(t)$ as shown in red in Fig. 3(a). Thus, the time domain interference terms to the 2nd user ($u = 2$), which are caused from the different time periods can be computed as:

$$i_2^{\text{Diff}}(t) = \sum_{l=0}^{\tau-1} x_1^{\#3}(t)\delta(t-l) + \sum_{l=L-\tau}^{L-1} x_3^{\#1}(t)\delta(t-l), \quad (16)$$

where l is a sample index. Second, the remaining samples of $x_1^{\#2}(t)$ and $x_3^{\#2}(t)$ are nearly orthogonal with $x_2^{\#2}(t)$, which are transmitted in the same time period. If there is no time offsets, $x_1^{\#2}(t)$, $x_2^{\#2}(t)$ and $x_3^{\#2}(t)$ are orthogonal. Then, the dot product of $x_1^{\#2}(t)$ and $x_2^{\#2}(t)$ can be expressed as:

$$\sum_{l=0}^{L-1} x_1^{\#2}(t)e^{-j2\pi lt/N} \cdot x_2^{\#2}(t)e^{-j2\pi lt/N} = 0, \quad (17)$$

thus,

$$\sum_{l=0}^{\tau-1} x_1^{\#2}(t)e^{-j2\pi lt/N} \cdot x_2^{\#2}(t)e^{-j2\pi lt/N} + \sum_{l=\tau}^{L-1} x_1^{\#2}(t)e^{-j2\pi lt/N} \cdot x_2^{\#2}(t)e^{-j2\pi lt/N} = 0, \quad (18)$$

and then,

$$\sum_{l=\tau}^{L-1} x_1^{\#2}(t)e^{-j2\pi lt/N} \cdot x_2^{\#2}(t)e^{-j2\pi lt/N} = \sum_{l=0}^{\tau-1} -x_1^{\#2}(t)e^{-j2\pi lt/N} \cdot x_2^{\#2}(t)e^{-j2\pi lt/N}. \quad (19)$$

Now, similarly, the time domain interference terms for $x_2^{\#2}(t)$, which are caused from the same time period can be computed as:

$$i_2^{\text{Same}}(t) = \sum_{l=0}^{\tau-1} -x_1^{\#2}(t)\delta(t-l) + \sum_{l=L-\tau}^{L-1} -x_3^{\#2}(t)\delta(t-l). \quad (20)$$

Finally, according to (16) and (20), we can write the total interference terms for $x_2^{\#2}(t)$ in the time domain as:

$$i_2^{\text{OFDM}}(t) = \sum_{l=0}^{\tau-1} x_1^{\#3}(t)\delta(t-l) + \sum_{l=L-\tau}^{L-1} x_3^{\#1}(t)\delta(t-l) + \sum_{l=0}^{\tau-1} -x_1^{\#2}(t)\delta(t-l) + \sum_{l=L-\tau}^{L-1} -x_3^{\#2}(t)\delta(t-l). \quad (21)$$

After removing the CP, we can rewrite (21) as:

$$i_2^{\text{OFDM}}(n) = \sum_{l=0}^{\tau-1} \big(-x_1^{\#2}(n) + x_1^{\#3}(n)\big)\delta(n-l) + \sum_{l=N-\tau+L_{\text{CP}}}^{N-1} \big(-x_3^{\#2}(n) + x_3^{\#1}(n)\big)\delta(n-l). \quad (22)$$

Similarly, the time domain interference for the 2nd symbol of user 1, $x_1^{\#2}(t)$, after removing the CP is:

$$i_1^{\text{OFDM}}(n) = \sum_{l=N-\tau+L_{\text{CP}}}^{N-1} \big(-x_2^{\#2}(n) + x_2^{\#1}(n)\big)\delta(n-l) + \sum_{l=N-2\tau+L_{\text{CP}}}^{N-1} \big(-x_3^{\#2}(n) + x_3^{\#1}(n)\big)\delta(n-l), \quad (23)$$

and for user 3, $x_3^{\#2}(t)$, is:

$$i_3^{\text{OFDM}}(n) = \sum_{l=0}^{2\tau-1} \big(-x_1^{\#2}(n) + x_1^{\#3}(n)\big)\delta(n-l) + \sum_{l=0}^{\tau-1} \big(-x_2^{\#2}(n) + x_2^{\#3}(n)\big)\delta(n-l). \quad (24)$$

Now, the frequency domain interference for the uth user can be rewritten using the discrete Fourier transform as I_u^{OFDM}:

$$I_1^{\mathrm{OFDM}} = \sum_{k=0}^{K-1} \sum_{n=N-\tau+L_{\mathrm{CP}}}^{N-1} \big(- x_2^{\#2}(n) + x_2^{\#1}(n) \big) e^{-j2\pi nk/N} + \sum_{k=0}^{K-1} \sum_{n=N-2\tau+L_{\mathrm{CP}}}^{N-1} \big(- x_3^{\#2}(n) + x_3^{\#1}(n) \big) \cdot e^{-j2\pi nk/N}, \tag{25}$$

$$I_2^{\mathrm{OFDM}} = \sum_{k=0}^{K-1} \sum_{n=0}^{\tau-1} \big(- x_1^{\#2}(n) + x_1^{\#3}(n) \big) e^{-j2\pi nk/N} + \sum_{k=0}^{K-1} \sum_{n=N-\tau+L_{\mathrm{CP}}}^{N-1} \big(- x_3^{\#2}(n) + x_3^{\#1}(n) \big) \cdot e^{-j2\pi nk/N}, \tag{26}$$

$$I_3^{\mathrm{OFDM}} = \sum_{k=0}^{K-1} \sum_{n=0}^{2\tau-1} \big(- x_1^{\#2}(n) + x_1^{\#3}(n) \big) e^{-j2\pi nk/N} + \sum_{k=0}^{K-1} \sum_{n=0}^{\tau-1} \big(- x_2^{\#2}(n) + x_2^{\#3}(n) \big) e^{-j2\pi nk/N}. \tag{27}$$

We can conclude that the CP only can reduce the interference in the front of L_{CP} sample time offsets as shown in (25), where $(L_{\mathrm{CP}} - \tau)$ error samples have been considered. When the interference is located in the final τ samples, CP-OFDM would no longer be robust to the ICI, as shown in (26) and (27), e.g. as τ or 2τ error samples are considered as the interference.

2) UFMC / OA-UFMC System ICI Analysis: Unlike CP-OFDM, the side-lobe attenuation of UFMC is much smaller due to the time domain filtering. The narrow band filter used at the transmitter can significantly reduce the interference caused by the time offset between the transmitting users. Similar to (21), we can write the time domain interference terms to uth user of UFMC as $i_u^{\mathrm{UFMC}}(t)$:

$$i_2^{\mathrm{UFMC}}(t) = \sum_{l=0}^{\tau-1} \big(- s_1^{\#2}(t) + s_1^{\#3}(t) \big) \delta(t-l) + \sum_{l=L-\tau}^{L-1} \big(- s_3^{\#2}(t) + s_3^{\#1}(t) \big) \delta(t-l), \tag{28}$$

thus, the frequency domain interference can be rewritten using the discrete Fourier transform as:

$$I_2^{\mathrm{UFMC}} = \sum_{k=0}^{K-1} \sum_{t=0}^{\tau-1} \big(- s_1^{\#2}(t) + s_1^{\#3}(t) \big) e^{-j2\pi tk/N} + \sum_{k=0}^{K-1} \sum_{t=L-\tau}^{L-1} \big(- s_3^{\#2}(t) + s_3^{\#1}(t) \big) e^{-j2\pi tk/N}. \tag{29}$$

Now, we define L_{T} as the transmitted signal tail length which is located at both the front and the end of the UFMC samples, and $L_{\mathrm{T}} = \frac{L_{\mathrm{F}}-1}{2}$. Then, the first term of (29) can be expanded as:

$$\sum_{k=0}^{K-1} \sum_{t=0}^{\tau-1} \big(- s_1^{\#2}(t) + s_1^{\#3}(t) \big) e^{-j2\pi tk/N} = \sum_{k=0}^{K-1} \left(\sum_{t=0}^{L_{\mathrm{T}}-1} \big(- s_1^{\#2}(t) + s_1^{\#3}(t) \big) + \sum_{t=L_{\mathrm{T}}}^{\tau-1} \big(- s_1^{\#2}(t) + s_1^{\#3}(t) \big) \right) \cdot e^{-j2\pi tk/N}, \tag{30}$$

and the second term of (29) can be expanded as:

$$\sum_{k=0}^{K-1} \sum_{t=L-\tau}^{L-1} \big(- s_3^{\#2}(t) + s_3^{\#1}(t) \big) e^{-j2\pi tk/N} = \sum_{k=0}^{K-1} \left(\sum_{t=L-\tau}^{L-L_{\mathrm{T}}-1} \big(- s_3^{\#2}(t) + s_3^{\#1}(t) \big) + \sum_{t=L-L_{\mathrm{T}}}^{L-1} \big(- s_3^{\#2}(t) + s_3^{\#1}(t) \big) \right) \cdot e^{-j2\pi tk/N}. \tag{31}$$

Note that, each filter is designed with the narrow bandwidth, using prototype Chebyshev or Hamming [20] designs to ensure that the magnitude of $b_u(t)$ at the band-edge should be very small. Now, the equation (29) can be summed from (30) and (31) as:

$$I_2^{\mathrm{UFMC}} = \sum_{k=0}^{K-1} \Big(\sum_{t=0}^{L_{\mathrm{T}}-1} \big(- s_1^{\#2}(t) + s_1^{\#3}(t) \big) + \sum_{t=L_{\mathrm{T}}}^{\tau-1} \big(- s_1^{\#2}(t) + s_1^{\#3}(t) \big) \Big) e^{-j2\pi tk/N} + \sum_{k=0}^{K-1} \Big(\sum_{t=L-\tau}^{L-L_{\mathrm{T}}-1} \big(- s_3^{\#2}(t) + s_3^{\#1}(t) \big) + \sum_{t=L-L_{\mathrm{T}}}^{L-1} \big(- s_3^{\#2}(t) + s_3^{\#1}(t) \big) \Big) e^{-j2\pi tk/N}. \tag{32}$$

Similarly, the interference of the 1st user in the frequency domain can be written as:

$$I_1^{\mathrm{UFMC}} = \sum_{k=0}^{K-1} \Big(\sum_{t=L-\tau}^{L-L_{\mathrm{T}}-1} \big(- s_2^{\#2}(t) + s_2^{\#1}(t) \big) + \sum_{t=L-L_{\mathrm{T}}}^{L-1} \big(- s_2^{\#2}(t) + s_2^{\#1}(t) \big) \Big) e^{-j2\pi tk/N} + \sum_{k=0}^{K-1} \Big(\sum_{t=L-2\tau}^{L-L_{\mathrm{T}}-1} \big(- s_3^{\#2}(t) + s_3^{\#1}(t) \big) + \sum_{t=L-L_{\mathrm{T}}}^{L-1} \big(- s_3^{\#2}(t) + s_3^{\#1}(t) \big) \Big) e^{-j2\pi tk/N}, \tag{33}$$

and for the 3^{th} user can be written as:

$$I_3^{\text{UFMC}} = \sum_{k=0}^{K-1}\Big(\sum_{t=0}^{L_{\text{T}}-1} \big(- s_1^{\#2}(t) + s_1^{\#3}(t)\big) + \sum_{L_{\text{T}}}^{2\tau-1} \big(- s_1^{\#2}(t) + s_1^{\#3}(t)\big)\Big)e^{-j2\pi tk/N} + \sum_{k=0}^{K-1}\Big(\sum_{t=0}^{L_{\text{T}}-1} \big(- s_2^{\#2}(t) + s_2^{\#3}(t)\big) + \sum_{L_{\text{T}}}^{\tau-1} \big(- s_2^{\#2}(t) + s_2^{\#3}(t)\big)\Big)e^{-j2\pi tk/N}. \tag{34}$$

The narrow band filter reduces the power amplitude at the band-edge, which directly reduces the ICI caused by the time offset overlapped samples. Note that, in terms of the multipath channel, this paper considers that the sum of the mean power values for all channel taps is equal to 1. The interference terms for the multipath channel can be easily computed as using $x_u^{\#}(t) \otimes h_u(t)$ or $s_u^{\#}(t) \otimes h_u(t)$ instead of $x_u^{\#}(t)$ or $s_u^{\#}(t)$ in the above equations, which can be used for the case of any of the multipath channels.

C. ISI Analysis Caused by Channel

This paper also considers the analysis of ISI when the length of channel impulse response in samples L_{H} is longer than L_{CP} or L_{F}.

1) CP-OFDM System ISI Analysis: Reference [21] proved that when $(L_{\text{H}} > L_{\text{CP}})$, a part of one signal will then be the ISI from the previous symbol and this causes interference at the tail of the channel impulse response that is not covered by the CP. Thus, the residual ISI of the uth user on the kth sub-carrier, after removing the CP in the frequency domain, can be expressed as $Z_u(k)$ [21]:

$$Z_u^{\text{OFDM}}(k) = \sum_{n=L_{\text{CP}}}^{L_{\text{H}}-1} x_{u-1}(n) \sum_{t=n}^{L_{\text{H}}-1} h_u(t)e^{-j2\pi(t-n)k/N} = \sum_{n=L_{\text{CP}}}^{L_{\text{H}}-1} x_{u-1}(n)e^{j2\pi nk/N} \sum_{t=n}^{L_{\text{H}}-1} h_u(t)e^{-j2\pi tk/N}, \tag{35}$$

then the PSD of ISI for the CP-OFDM system can be determined as P_{ISI}:

$$\begin{aligned} P_{\text{ISI}u}^{\text{OFDM}}(k) &= \mathbb{E}\left(Z_u^{\text{OFDM}}(k)Z_u^{\text{OFDM}*}(k)\right) \\ &= \mathbb{E}\left(x_{u-1}(n)x_{u-1}^*(n)\right)e^{-j2\pi(n-n)k/N} \\ &\cdot \sum_{n=L_{\text{CP}}}^{L_{\text{H}}-1}\sum_{t=n}^{L_{\text{H}}-1} h_u(t)e^{-j2\pi tk/N} \\ &\cdot \sum_{n=L_{\text{CP}}}^{L_{\text{H}}-1}\sum_{t=n}^{L_{\text{H}}-1} h_u^*(t)e^{-j2\pi tk/N} \\ &= \sigma^2 \sum_{n=L_{\text{CP}}}^{L_{\text{H}}-1}\left|\sum_{t=n}^{L_{\text{H}}-1} h_u(t)e^{-j2\pi tk/N}\right|^2. \end{aligned} \tag{36}$$

2) UFMC System ISI Analysis: Following a similar analysis to the CP-OFDM system, the residual ISI of the uth user on the kth sub-carrier for UFMC is:

$$\begin{aligned} Z_u^{\text{UFMC}}(k) &= \sum_{n=L_{\text{T}}}^{L_{\text{H}}-1} s_{u-1}(n)e^{j2\pi nk/N} \sum_{t=n}^{L_{\text{H}}-1} h_u(t)e^{-j2\pi tk/N} \\ &= \sum_{n=L_{\text{T}}}^{L_{\text{H}}-1} x_{u-1}(n)b_{u-1}(n)e^{j2\pi nk/N} \sum_{t=n}^{L_{\text{H}}-1} h_u(t)e^{-j2\pi tk/N}. \end{aligned} \tag{37}$$

Thus, the PSD of ISI for the UFMC system can be determined as:

$$\begin{aligned} P_{\text{ISI}u}^{\text{UFMC}}(k) &= \mathbb{E}\left(x_{u-1}(n)x_{u-1}^*(n)\right)e^{-j2\pi(n-n)k/N} \\ &\cdot \sum_{n=L_{\text{T}}}^{L_{\text{H}}-1}\sum_{t=n}^{L_{\text{H}}-1} b_u(t)h_u(t)e^{-j2\pi tk/N} \\ &\cdot \sum_{n=L_{\text{T}}}^{L_{\text{H}}-1}\sum_{t=n}^{L_{\text{H}}-1} b_u^*(t)h_u^*(t)e^{-j2\pi tk/N} \\ &= \sigma^2 \sum_{n=L_{\text{T}}}^{L_{\text{H}}-1}\left|\sum_{t=n}^{L_{\text{T}}-1} b_u(t)h_u(t)e^{-j2\pi tk/N}\right|^2. \end{aligned} \tag{38}$$

D. SINR Analysis and Achievable Rate

The SINR of the received signal on kth sub-carrier can be defined as $\rho_u(k)$:

$$\rho_u(k) = \frac{\mathbb{E}[X_u(k)^2]}{\sigma^2 + \mathbb{E}[I_u(k)^2] + P_{\text{ISI}u}(k)}, \tag{39}$$

where $\mathbb{E}[X_u(k)^2]$ denotes the transmitted signal power. Inserting (25), (26), (27) and (36) into (39), the closed-form expression of SINR for the uth user CP-OFDM can be expressed as in (40). Now, inserting (32), (33), (34) and (38) into (39), the closed-form expression of SINR for the uth user UFMC can be expressed as in (41). Now, we can compute an estimate of the achievable rate $R_u(k)$ for the kth sub-carrier of the uth user based on our SINR equations as:

$$R_u^{\text{OFDM}}(k) = \log_2(1 + \rho_u^{\text{OFDM}}(k)), \tag{42}$$

$$R_u^{\text{UFMC}}(k) = \log_2(1 + \rho_u^{\text{UFMC}}(k)). \tag{43}$$

E. BER Analysis

This paper now considers the performance for a 4PSK modulation scheme. As in [22] and [23], we can express the theoretical BER values for the time offset model under the AWGN channel as:

$$P_{4\text{PSK}u}^{\text{OFDM}} = \frac{1}{2}\text{erfc}\left(\sqrt{\overline{\rho_u^{\text{OFDM}}}/N_{\text{bs}}}\right), \tag{44}$$

$$P_{4\text{PSK}u}^{\text{UFMC}} = \frac{1}{2}\text{erfc}\left(\sqrt{\overline{\rho_u^{\text{UFMC}}}/N_{\text{bs}}}\right), \tag{45}$$

where $\text{erfc}(\cdot)$ represents the complementary error function, $\overline{\rho_u}$ is the average value of SINR and N_{bs} is the number of bits

$$\rho_u^{\mathrm{OFDM}}(k) = \frac{\mathbb{E}[X_u(k)^2]}{\sigma^2 + \mathbb{E}[(I_u^{\mathrm{OFDM}}(k))^2] + \sigma^2 \sum_{n=L_{\mathrm{CP}}}^{L_{\mathrm{H}}-1} \left| \sum_{t=n}^{L_{\mathrm{H}}-1} h_u(t) e^{-j2\pi tk/N} \right|^2}. \tag{40}$$

$$\rho_u^{\mathrm{UFMC}}(k) = \frac{\mathbb{E}[S_u(k)^2]}{\sigma^2 + \mathbb{E}[(I_u^{\mathrm{UFMC}}(k))^2] + \sigma^2 \sum_{n=L_{\mathrm{T}}}^{L_{\mathrm{H}}-1} \left| \sum_{t=n}^{L_{\mathrm{T}}-1} b_u(t) h_u(t) e^{-j2\pi tk/N} \right|^2}. \tag{41}$$

per sample. For the Rayleigh multipath channel, according to [22] and [23], the BER equations are given:

$$P_{4\mathrm{PSK}u}^{\mathrm{OFDM}} = \frac{1}{2}\mathrm{erfc}\left(1 - \sqrt{\frac{\overline{\rho_u^{\mathrm{OFDM}}}/N_{\mathrm{bs}}}{1 + \overline{\rho_u^{\mathrm{OFDM}}}/N_{\mathrm{bs}}}}\right), \tag{46}$$

$$P_{4\mathrm{PSK}u}^{\mathrm{UFMC}} = \frac{1}{2}\mathrm{erfc}\left(1 - \sqrt{\frac{\overline{\rho_u^{\mathrm{UFMC}}}/N_{\mathrm{bs}}}{1 + \overline{\rho_u^{\mathrm{UFMC}}}/N_{\mathrm{bs}}}}\right). \tag{47}$$

For the higher order modulation scheme required in PCC-OFDM, i.e. 16-QAM, to achieve a spectral efficiency of $\eta = 2$ bit/sec/Hz, the standard theoretical BER equations can be found in [22]. Inserting our SINR equations into the formulas given in [22] allows us to compute the 16-QAM theoretical BER values.

V. NUMERICAL RESULTS

In this section, various simulations are conducted to confirm our theoretical analysis. The common simulation parameters are listed in Table I. Each MTC user's transmission occupies 13 sub-carriers in the frequency domain, and the users are spaced by 2 blank sub-carriers. We set the normalised cut-off frequency to $f_{\mathrm{cf}} = 0.18$, which is wider than the ratio between the number of sub-carriers per user K and the total number of available sub-carriers N, $\gamma_{\mathrm{ro}} = 13/128 = 0.1016$. A_{SL} is the side-lobe attenuation and A_{PB} is the passband ripple. In the BER simulations, we elected to measure the middle user's performance, e.g. when $U = 3$, we measure the 2nd user and when $U = 7$, we measure the 4^{th} user.

A. PSD Performance

In terms of analysing the ICI caused by the time offsets, this paper now measures the power spectral density performance of the candidate waveform designs. The side-lobe behaviour of the OFDM system with $U = 7$ users is shown in Fig. 4. Here we assume each user has 13 sub-carriers over the 1.25 MHz channel with a 128-point FFT, i.e. the 4th OFDM symbol shares sub-carriers from 55 to 67 and with 2 blank sub-carriers between the adjacent users, the 3rd user shares sub-carriers from 40 to 52 and the 5th user shares from 70 to 82 etc. The OFDM spectrum has high side-lobe levels resulting from the rectangular time domain pulse shape. This causes ICI and performance degradation, and the orthogonality between sub-carriers collapses. The high OFDM side-lobes significantly affect nearby sub-carriers, especially for the adjacent users, e.g. the 4th user interferes with the 3rd and 5th users. The side-lobe attenuation in the roll-off region lies between -11 dB and -25 dB for the 3rd and 5th users, which are placed at the adjacent sub-bands. Moreover, side-lobe attenuation for the 2nd and 6th user bands reduces from -25 dB to -30 dB, but this still can cause significant interference.

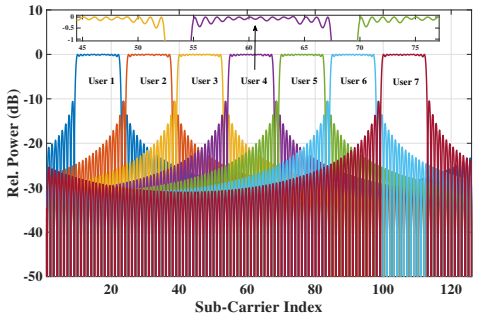

Fig. 4. Superimposed Spectra of 7 Different OFDM Resource Users, $N = 128$.

The PSD performance of CP-OFDM, PCC-OFDM and UFMC with different types of FIR filters is shown in Fig. 5(a). Firstly, both UFMC and PCC-OFDM significantly reduce the side-lobe level compared to CP-OFDM. Among these, PCC-OFDM provides the best ICI protection due to its very rapid side-lobe roll-off. However, it increases the passband ripple from -5 dB to 5 dB. The reason could be the pairs of sub-carriers have a relative weighting of $+1$, 1. Therefore, in these receivers, pairs of sub-carriers should be combined by weighting prior to summation. Secondly, in terms of the Dolph-Chebyshev filter, compared with $A_{\mathrm{SL}} = 64$ dB, the PSD performance of $A_{\mathrm{SL}} = 40$ dB is better, as it achieves a slightly lower side-lobe attenuation in the roll-off region. Both the Dolph-Chebyshev filter with $A_{\mathrm{SL}} = 40$ dB and the Hamming filter present better frequency roll-off performance than the Blackman filter. Moreover, there are no significant differences between Dolph-Chebyshev and Hamming filters. Thus, this paper will focus on the Hamming filter in the next simulations.

The PSD performance of IIR-UFMC is shown in Fig. 5(b). In terms of a fair comparison, we truncated the lengths of all IIR filtered signal outputs equal to L. The normalised cut-off frequency is set to $f_{\mathrm{cf}} = 0.18$, which is much wider than $\gamma_{\mathrm{ro}} = 0.1016$ to achieve an almost linear phase in passband. We assume the available sub-carriers for transmission are from 58 to 70, i.e. 13 sub-carriers. Fig. 5(b) clearly shows that

TABLE I
COMMON SIMULATION PARAMETERS.

Simulation Parameters							
Uplink Bandwidth 1.25 MHz	No. of FFT (N) 128	Sub-carriers per user (K) 13	Total Users (U) 3 or 7	CP Length (L_{CP}) 30	Filter Length (L_{F}) 31	Channel Length (L_{H}) 10 or 70	Modulation Scheme 4PSK

Filter Parameters						
FIR Filter			IIR Filter			
FIR Window	Normalised cut-off frequency (f_{cf})	Side-lobe Attenuation (A_{SL})	Type of Filter	f_{cf}	Filter Order	Passband Ripple (A_{PB})
Hamming	0.18	40 or 64 (dB)	Chebyshev Type I	0.18	4, 8, 12	0.15 (dB)

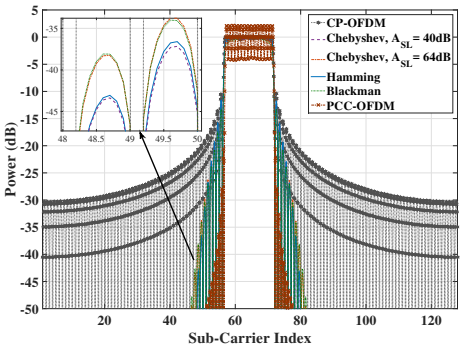

(a) CP-OFDM, UFMC with Different Filters, PCC-OFDM

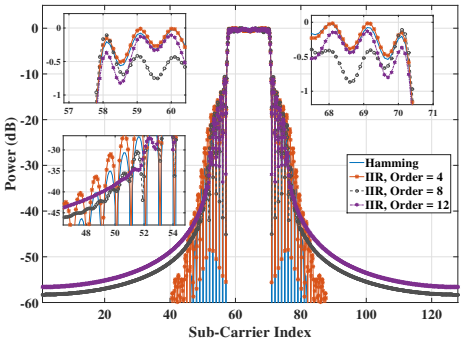

(b) IIR-UFMC, Truncating the Filter Outputs to L Samples.

Fig. 5. PSD Performance in the Side-lobes Region.

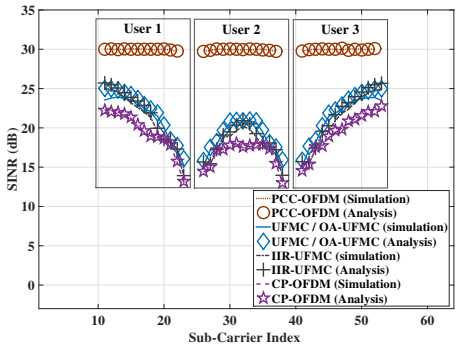

(a) SINR Degradation Performance

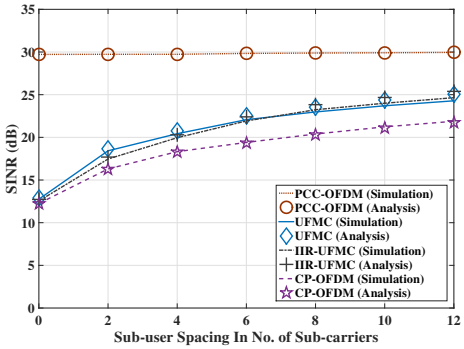

(b) SINR Performance with Blank Sub-carriers

Fig. 6. SINR Performance, AWGN (SNR =30 dB), $N = 128$, $L_{\mathrm{CP}} = 30$, $L_{\mathrm{F}} = 31$, $L_{\mathrm{Or}} = 4$, $\tau = 50$, $U = 3$.

IIR filters with order of 8 and 12 provide slightly superior frequency roll-off performance at the centre of adjacent sub-carriers (from 48 to 58) to both the FIR Hamming window and IIR with order of 4. However, when increasing the filter order, the truncated L samples will no longer accurately represent the original signal and also they introduce increased computational cost. Therefore, this paper will consider the Chebyshev Type I IIR filter with order 4 for the IIR-UFMC system in the following simulations.

B. SINR and Achievable Rate Performance

The SINR performance over the AWGN channel for 3 users with a signal to noise ratio (SNR) of 30 dB is shown in Fig. 6(a) and we assume τ is a 50 sample time offset, which is larger than $L_{\mathrm{CP}} = 30$ or $L_{\mathrm{F}} = 31$. The theoretical SINR analysis values are computed from (40) and (41), which perfectly match with the simulations. The 1st user occupies sub-carriers from 11 to 23, sub-carriers 26 to 38 are for the 2nd user and 41 to 53 are for the 3rd user. Note in Fig. 6(a) how the SINR performance degrades due to interference between users 1&2 and also 2&3 for OFDM, UFMC and IIR-UFMC. From Fig. 6(a), we notice that first, compared with OFDM, UFMC and IIR-UFMC, PCC-OFDM presents the best performance due to its fast frequency roll-off performance (the PSD results as shown in Fig 5(a)). The rapid frequency roll-off of PCC-OFDM directly reduces the interference caused by the adjacent sub-bands or users. Second, the nearby sub-carriers of both OFDM, UFMC, and IIR-UFMC are significantly affected by ICI, especially for the second user. Third, both UFMC and IIR-UFMC can perform slightly better than OFDM (about 3.5 dB higher SINR), but they still have an inferior SINR to PCC-OFDM. There is no significant performance difference between UFMC and IIR-UFMC.

The impact of the number of zero sub-carriers in the frequency domain between each user is shown in Fig. 6(b). When increasing the number of blank sub-carriers at the user band-edge, the SINR performance of both CP-OFDM, UFMC and IIR-UFMC improves significantly at the cost of reducing the available bandwidth for data transmission. Moreover, if the sub-user spacing is 4 blank sub-carriers, UFMC achieves about 0.5 dB higher SINR than IIR-UFMC and about 2.6 dB higher SINR than CP-OFDM. PCC-OFDM still provides the best performance compared with the other schemes. It can also be seen that the result from the analysis match very well with the simulations.

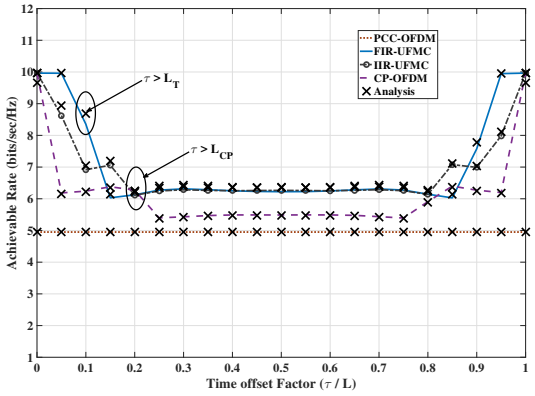

Fig. 7. Achievable Rate Performance, AWGN (SNR = 30 dB), $U = 3$, $N = 128$, $L_{\mathrm{CP}} = 30$, $L_{\mathrm{F}} = 31$, $L_{\mathrm{T}} = 15$, $U = 3$.

The achievable rate performance with the time offset factor (τ/L) is shown in Fig. 7. The theoretical achievable rate values are computed from (42) and (43), and the results from our derived expressions and the simulations match perfectly. It can be seen that firstly, PCC-OFDM provides the poorest spectral efficiency, even though it achieves the highest SINR performance in Fig. 6. Secondly, with increasing τ, the achievable rate performance of UFMC, IIR-UFMC and OFDM significantly reduces due to the ICI. However, when $\tau = L = 158$ samples, there is no significant achievable rate degradation as there are no relative time offsets between the adjacent users. Thirdly, if there is a small time offset, i.e. $\tau = 5\%$ of the transmitted symbol length, both UFMC and IIR-UFMC are more robust to ICI compared with OFDM. In detail, the achievable rate degradation for UFMC and IIR-UFMC significantly reduces when $\tau > 10\%$ (or 15 samples) of the transmitted symbol length, which is approximately the window tail length L_{T}. The achievable rate degradation for OFDM starts with when $\tau > 5\%$ of the transmitted symbol length and then stays at a constant value of 6.3 bit/sec/Hz until $\tau > 20\%$ (or 30 samples), which is approximately the CP length. Fourthly, if $\tau > 20\%$ of the transmitted symbol length, both UFMC, IIR-UFMC and OFDM provide an approximately constant achievable rate. Both FIR-UFMC and IIR-UFMC achieve 1 bit/sec/Hz higher achievable rate than OFDM. Finally, there is no significant difference between FIR-UFMC and IIR-UFMC when $\tau > 20\%$.

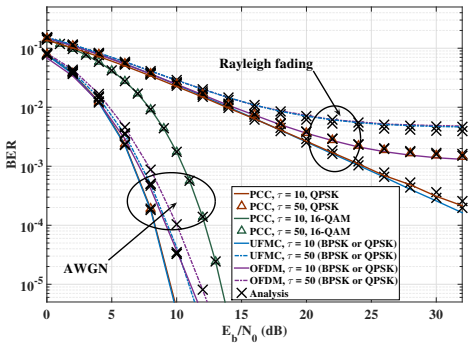

(a) Approximate BER Performance, $L_{\mathrm{H}} = 10$.

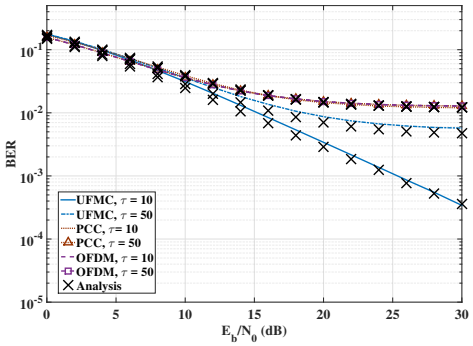

(b) Approximate BER and ISI Performance, $L_{\mathrm{H}} = 70$.

Fig. 8. BER Performance for AWGN and Rayleigh Multipath Channel, $U = 3$, $N = 128$, $L_{\mathrm{CP}} = 30$, $L_{\mathrm{F}} = 31$, $\eta = 1$ or 2 bit/sec/Hz.

C. BER Performance

The average BER for the OFDM, UFMC and PCC-OFDM systems for AWGN and Rayleigh fading channels is shown in Fig. 8(a). The time offset scenarios of $\tau = 10$ or $\tau = 50$ samples are considered. The theoretical BER results are obtained using the proposed equations as (44), (45), (46) and (47). Again, the agreement between the analytical and simulation results is clear. The BER results show similar trends to the previous SINR results. Firstly, there is no significant BER degradation for PCC-OFDM even if there is a 50 sample time offset, which means PCC-OFDM can significantly mitigate against the ICI. However, if we consider the spectral efficiency as $\eta = 2$ bit/sec/Hz, PCC-OFDM will no longer provide superior BER performance due to the requirement to use a higher order modulation scheme, i.e. 16QAM. Secondly, when $\tau < L_{\mathrm{CP}}$ or $L_{\mathrm{F}} - 1$, there is no significant BER degradation for UFMC, especially when the time offset is less than 15 samples. Even when $\tau = 50$, UFMC saves about 1.1 dB E_{b}/N_0 compared with OFDM at a BER of 10^{-4} in the AWGN channel. Fig. 8(a) also shows that if for the multipath channel $L_{\mathrm{H}} = 10$ and $\tau = 10$, UFMC saves about 5 dB E_{b}/N_0 at the BER of $10^{-2.9}$. If the τ increases to 50 samples, the BER performance of both UFMC and OFDM will degrade to the same curve.

The approximate BER for the OFDM, UFMC and PCC-OFDM systems in a Rayleigh fading channel with $L_{\mathrm{H}} = 70$ channel taps is shown in Fig. 8(b). The theoretical ISI interfer-

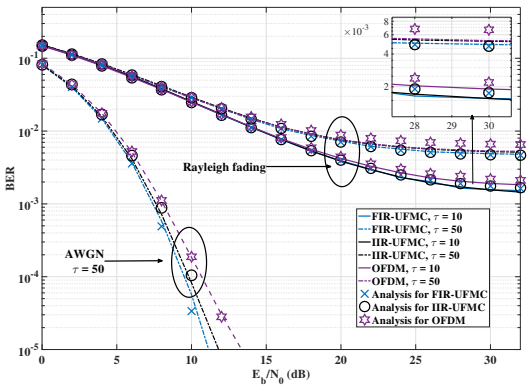

Fig. 9. Approximate BER Performance for UFMC with FIR and IIR Filter When Receiving $U = 7$ Users, $L_{\rm H} = 10$.

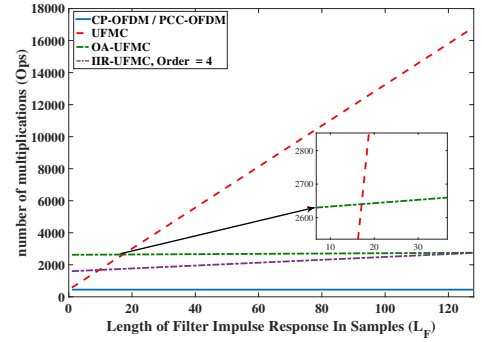

(a) Comparison of Computational Complexity Performance.

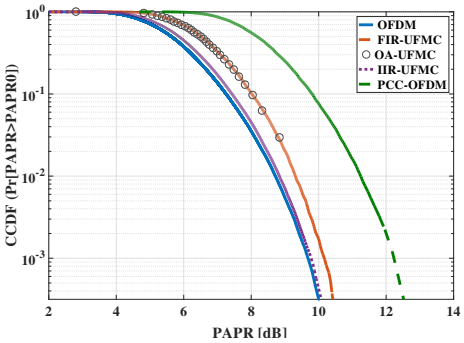

(b) The peak-to-average power ratio (PAPR) Performance.

Fig. 10. System Performance of Computational Complexity and PAPR.

ence is computed using (36) and (38), and simulations closely match with the analytical results. It can be seen that UFMC is more robust to very dispersive multipath channels compared with CP-OFDM and PCC-OFDM, especially when τ is small. Fig. 8(b) also shows that if $L_{\rm H}$ is much longer than $L_{\rm CP}$, ISI becomes the dominant interference for both OFDM and PCC-OFDM systems. In this case, the ICI caused by the time offset is somewhat smaller than ISI.

Now we measure the BER performance of IIR-UFMC, using the Chebyshev Type I filter with order of 4 and $f_{\rm cf} = 0.18$. Here, we increase the number of transmitting users to $U = 7$ and measure the $4^{\rm th}$ user's performance. The competitive BER performance for UFMC with the FIR and IIR filters is shown in Fig. 9. The analytical values are computed as before, with the interference analysed using the sub-carriers from the adjacent users. Fig. 9 shows that the BER performance of IIR-UFMC is slightly less than for the FIR-UFMC. The reason is that we truncated the output length of IIR to L in order to ensure a fair comparison. Compared with OFDM, the BER performance of IIR-UFMC is significantly improved, especially for the Rayleigh multipath channel with the short impulse response $L_{\rm H} = 10$ taps and small $\tau = 10$ samples. Again, the theoretical analysis closely matches with the Monte Carlo simulations.

D. Computational Complexity and PAPR

The relative computational complexity is shown in Fig. 10(a) using (11), (12), (14) and (15). Both CP-OFDM and PCC-OFDM require significantly fewer operations than time domain UFMC and OA-UFMC. When $L_{\rm F} < 17$ samples, the standard UFMC requires fewer operations than OA-UFMC. As $L_{\rm F}$ increases, the number of operations for UFMC significantly increases. In this case, OA-UFMC reduces the computational complexity significantly for larger values of $L_{\rm F}$. IIR-UFMC, with a filter order of 4, only slightly increases the computational complexity compared with OFDM and PCC-OFDM, but it is significantly better than IIR-UFMC.

The peak-to-average power ratio (PAPR) performance is shown in Fig. 10(b). Both FIR/OA-UFMC, IIR-UFMC and PCC-OFDM increase the PAPR compared with OFDM. IIR-UFMC only slightly increases the PAPR when compared with OFDM, but it is still significantly better than the other waveforms. The PAPR of PCC-OFDM is about 2.1 dB higher than OFDM and 1.95 dB higher than FIR-UFMC (or OA-UFMC) at a complementary cumulative distribution function (CCDF) value of 10^{-2}. The reason could be that the complementary cumulative distribution function of PAPR is derived for PCC-OFDM with a Gaussian approximation and is shown to have a prolonged tail. Its characteristic as a matched windowing scheme is shown in Fig. 5(a). Thus, for PCC-OFDM, the side-lobe reduction comes at the cost of a slightly higher PAPR. This will require a higher power amplifier for the same signal coverage, assuming that the PAPR leads to an increased amplifier back-off.

The system performance with different values of $L_{\rm F}$ or $L_{\rm CP}$ over the AWGN channel is shown in Table II. Here we assume $N = 128$, $U = 7$ users and our aim is to achieve a BER of 10^{-3}. First, OFDM always requires the lowest number of operations (448 Ops.) but it needs the highest of $E_{\rm b}/N_0$. Second, PCC-OFDM provides the best performance in terms of saving $E_{\rm b}/N_0$ and lowest computational complexity at the cost of high PAPR and halving the spectral efficiency. Third, with increasing $L_{\rm F}$, FIR-UFMC, OA-UFMC and IIR-UFMC can reduce the required $E_{\rm b}/N_0$ at the cost of high computational complexity. Compared with the FIR-UFMC, OA-UFMC provides a similar performance and significantly reduces the computational complexity (i.e. when $L_{\rm F} = 31$, it saves 1762 Ops. and when $L_{\rm F} = 51$, it saves 4320 Ops.). IIR-

TABLE II
SYSTEM PERFORMANCE VS. COMPUTATIONAL COMPLEXITY.

Length of Filter Impulse Response ($L_{\mathrm{F}} = 31$) or Length of CP ($L_{\mathrm{CP}} = L_{\mathrm{F}} - 1 = 30$)				Length of Filter Impulse Response ($L_{\mathrm{F}} = 51$) or Length of CP ($L_{\mathrm{CP}} = L_{\mathrm{F}} - 1 = 50$)			
Waveform Design	BER	E_{b}/N_0 (dB)	Computational Complexity No. of Operations (Ops.)	Waveform Design	BER	E_{b}/N_0 (dB)	Computational Complexity No. of Operations (Ops.)
OFDM	10^{-3}	8.11	448	OFDM	10^{-3}	7.84	448
PCC-OFDM	10^{-3}	6.69	448	PCC-OFDM	10^{-3}	6.69	448
FIR-UFMC	10^{-3}	7.42	4416	FIR-UFMC	10^{-3}	7.36	6976
OA-UFMC	10^{-3}	7.42	2654	OA-UFMC	10^{-3}	7.36	2674
IIR-UFMC	10^{-3}	7.63	1870	IIR-UFMC	10^{-3}	7.58	2050

UFMC significantly reduces the computational complexity, although it requires a slightly higher E_{b}/N_0 compared with FIR-UFMC or OA-UFMC, but it is still lower than OFDM.

This paper has simulated the system performance (i.e. PSD, complexity, achievable rate, SINR, BER and PAPR) over several waveform designs, now we briefly discuss the overall system performance. If the aim is only to achieve the best BER performance (i.e. the BER of 10^{-3}), PCC-OFDM could be the best choice due to its lowest E_{b}/N_0 requirement. If we aim to achieve superior BER, achievable rate, and PAPR performance, the proposed OA-UFMC method could be the best solution due to its lower computational complexity compared with FIR-UFMC. If we aim for better BER, achievable rate and PAPR performance and combine this with the lowest computational complexity, the proposed IIR-UFMC method is superior.

VI. CONCLUSION

This paper has provided a complete time offset performance analysis for both CP/PCC-OFDM and UFMC systems and shown how the high OFDM spectral side-lobes cause significant interference for an asynchronous data transmission. PCC-OFDM achieves the required fastest frequency roll-off performance, resulting in good SINR performance at the costs of poor spectral efficiency and high PAPR. FIR-UFMC offers superior spectral efficiency, SINR, achievable rate and BER but at the cost of high computational complexity. Thus none of OFDM, PCC-OFDM or FIR-UFMC can be recommended as appropriate waveforms to select for MTC. IIR-UFMC, with its lower level of spectral side-lobes, offers an acceptable compromise on computational complexity, SINR, achievable rate, PAPR and BER performance. This detailed trade-off between system performance and computational complexity has thus shown IIR-UFMC to be a potentially attractive waveform design for the massive machine type 5G scenario to effectively support the required low data rates, low energy consumption and low latency signal transmissions.

REFERENCES

[1] V. W. S. Wong *et al*, *Key Technologies for 5G Wireless Systems*, 1st Edition edition, Ed. Cambridge university press, 2017.

[2] E. Hossain *et al*, "Evolution toward 5G multi-tier cellular wireless networks: An interference management perspective," *IEEE Wireless Communications*, vol. 21, no. 3, pp. 118–127, June 2014.

[3] J. G. Andrews *et al*, "What will 5G be?" *IEEE J. Sel. Areas Commun.*, vol. 32, no. 6, pp. 1065–1082, June 2014.

[4] E. Hossain and M. Hasan, "5G cellular: key enabling technologies and research challenges," *IEEE Instrum. Meas. Mag.*, vol. 18, no. 3, pp. 11–21, June 2015.

[5] M. O. Pun *et al*, "Maximum-likelihood synchronization and channel estimation for OFDMA uplink transmissions," *IEEE Trans. Commun.*, vol. 54, no. 4, pp. 726–736, April 2006.

[6] G. Wunder *et al*, "5GNOW: non-orthogonal, asynchronous waveforms for future mobile applications," *IEEE Commun. Mag.*, vol. 52, no. 2, pp. 97–105, February 2014.

[7] F. Schaich and T. Wild, "Waveform contenders for 5G, OFDM vs. FBMC vs. UFMC," in *International Symposium on communications, Control and Signal Processing (ISCCSP)*, May 2014, pp. 457–460.

[8] J. Armstrong, "Analysis of new and existing methods of reducing intercarrier interference due to carrier frequency offset in OFDM," *IEEE Trans. Commun.*, vol. 47, no. 3, pp. 365–369, Mar 1999.

[9] B. Farhang-Boroujeny, "OFDM versus filter bank multicarrier," *IEEE Signal Process. Mag.*, vol. 28, no. 3, pp. 92–112, May 2011.

[10] F. Schaich, T. Wild, and Y. Chen, "Waveform contenders for 5G - suitability for short packet and low latency transmissions," in *IEEE Vehicular Technology Conference (VTC Spring)*, May 2014, pp. 1–5.

[11] S. Wang, J. Armstrong, and J. S. Thompson, "Waveform performance for asynchronous wireless 5G uplink communications," in *2016 IEEE 27th Annual International Symposium on Personal, Indoor, and Mobile Radio Communications (PIMRC)*, Sept 2016, pp. 1–6.

[12] *3GPP, TSG-RAN WG184b, R1-162199, Waveform Candidates*, URL:http://www.ee.iitm.ac.in/ giri/pdfs/EE5141/R1-162199-Waveform-Candidates.docx.

[13] X. Wang *et al*, "Universal filtered multi-carrier with leakage-based filter optimization," in *European Wireless Conference, Proceedings of European Wireless*, May 2014, pp. 1–5.

[14] A. Aminjavaheri *et al*, "Impact of timing and frequency offsets on multicarrier waveform candidates for 5G," in *IEEE Signal Processing and Signal Processing Education Workshop (SP/SPE)*, Aug 2015, pp. 178–183.

[15] S. M. Kang *et al*, "Timing-offset-tolerant universal- filtered multicarrier passive optical network for asynchronous multiservices-over-fiber," *IEEE J. Opt. Commun. Netw.*, vol. 8, no. 4, pp. 229–237, April 2016.

[16] M. J. Narasimha, "Modified overlap-add and overlap-save convolution algorithms for real signals," *IEEE Signal Process. Lett.*, vol. 13, no. 11, pp. 669–671, Nov 2006.

[17] S. Holford and P. Agathoklis, "The use of model reduction techniques for designing IIR filters with linear phase in the passband," *IEEE Trans. Signal Process.*, vol. 44, no. 10, pp. 2396–2404, Oct 1996.

[18] R. Losada and V. Pellisier, "Designing IIR filters with a given 3-dB point," *IEEE Signal Process. Mag.*, vol. 22, no. 4, pp. 95–98, July 2005.

[19] B. Mulgrew, P. M. Grant, and J. S. Thompson, *Digital Signal Processing: Concepts and Applications*, 2nd Edition edition, Ed. Palgrave Macmillan, 2002.

[20] K. K. Wojcicki and K. K. Paliwal, "Importance of the dynamic range of an analysis window function for phase-only and magnitude-only reconstruction of speech," in *2007 IEEE International Conference on Acoustics, Speech and Signal Processing - ICASSP '07*, vol. 4, April 2007, pp. IV–729–732.

[21] W. Henkel *et al*, "The cyclic prefix of OFDM/DMT - an analysis," in *in Proc. International Seminar on Broadbond Communicalions, Access, Transmission, Networking, Zurich*, 2002, pp. 22–1–22–3.

[22] F. Adachi, "BER analysis of 2PSK, 4PSK, and 16QAM with decision feedback channel estimation in frequency-selective slow Rayleigh fading," *IEEE Trans. Veh. Technol.*, vol. 48, no. 5, pp. 1563–1572, Sep 1999.

[23] S. Wang and J. S. Thompson, "Performance analysis of VC receiver systems for M2M communications using orthogonal frequency-division multiple access," *IET Communications*, vol. 10, no. 16, pp. 2061–2070, 2016.